Nuclear Instruments and Methods in Physics Research B 267 (2009) 45–52

Contents lists available at ScienceDirect

Nuclear Instruments and Methods in Physics Research B

journal homepage: www.elsevier.com/locate/nimb

Electron inelastic mean free paths in biological matter based on dielectric theory and local-field corrections

D. Emfietzoglou [a], I. Kyriakou [a], I. Abril [b], R. Garcia-Molina [c], I.D. Petsalakis [d], H. Nikjoo [e], A. Pathak [f,*]

[a] Medical Physics Laboratory, University of Ioannina Medical School, Ioannina 451 10, Greece
[b] Departament de Física Aplicada, Universitat d'Alacant, Apartat 99, E-03080 Alacant, Spain
[c] Departamento de Física-CIOyN, Universidad de Murcia, Apartado 4021, E-30080 Murcia, Spain
[d] Theoretical and Physical Chemistry Institute, The National Hellenic Research Foundation, Athens 116 35, Greece
[e] Department of Medical Radiation Physics, Karolinska Institute, Box 260, SE-171 76 Stockholm, Sweden
[f] School of Physics, University of Hyderabad, Central University (P.O), Hyderabad, Andra Pradesh 500 046, India

ARTICLE INFO

Article history:
Received 17 August 2008
Received in revised form 28 October 2008
Available online 20 November 2008

PACS:
34.80.Dp
61.85.+p
77.22.Ch

Keywords:
Inelastic mean free path
Dielectric theory
Local-field corrections
Biological materials
Water

ABSTRACT

The inelastic mean free path (IMFP) of electrons with energies up to a few keV is calculated from the dielectric electron-gas theory for densities corresponding to those of biological matter. The effect of the many-body local-field correction on the Lindhard dielectric response function is examined using some of the available analytical approximations to its static limit. We have tested the performance of several Hubbard-type local-field corrections along with the formula proposed by Corradini and co-workers [M. Corradini, R. Del Sole, G. Onida, M. Palumno, Phys. Rev. B 57 (1998) 14569] which is extensively used in connection with the exchange-correlation kernel of time-dependent density functional theory. It is shown that the Lindhard dielectric function provides reasonable estimates of electron IMFPs below about 50 eV, where the majority of semi-empirical dielectric calculations based on the extended-optical-data methodology fail. The use of LFC results in a sizeable reduction of the IMFP which, at low energies, may reach ~20%.

1. Introduction

Electron inelastic scattering in condensed matter plays a fundamental role in many applied fields ranging from material and surface science to medical physics. Perhaps the single most important quantity is the electron inelastic mean free path (IMFP), which represents the mean distance between successive inelastic collisions. For example, in surface sensitive techniques, such as X-ray photoelectron spectroscopy (XPS) or Auger-electron spectroscopy (AES), IMFP is an indispensable input parameter for the quantitative interpretation of the results [1]. On the other hand, since secondary electrons represent the main source of radiation damage following X-ray (or charge particle) irradiation, knowledge of electron IMFPs is an essential step towards predicting radiation effects in both living and non-living matter [2,3]. Finally, IMFPs are important in the study of hot-electron lifetimes and transport in electronic devices under high-electric fields [4].

In the above applications, IMFP needs to be known over a broad range of electron energies, typically, from several keV down to the band-gap energy (or the Fermi energy for metals). However, in this low-energy range Bethe's optical approximation (essentially a high-energy approximation) becomes gradually invalid and, therefore, the momentum-dependent dielectric response function should be used. Lindhard [5] was the first to provide an analytic expression for the dielectric response function of the homogeneous electron-gas (HEG) within the so-called random-phase-approximation (RPA). For realistic materials, however, first-principle calculations of their dielectric response function are complicated because they involve a description of their band-structure [6–9].

Presently, the most practical approach to IMFP calculations which combines low computational effort and reasonable accuracy, and is applicable over a wide electron range and to any type of material (metal, semiconductor, insulator), is the extended-optical-data methodology [10,11]. In this approach one uses experimental "optical" data (i.e. at zero momentum-transfer) to first describe the dependence of the dielectric function on energy transfer and subsequently implements an "extension" (or dispersion) scheme to incorporate the dependence on momentum-transfer. The method has

* Corresponding author. Tel.: +91 40 23010181/23134316; fax: +91 40 23010181/23010227.
E-mail addresses: appsp@uohyd.ernet.in, iba2007@uohyd.ernet.in (A. Pathak).

0168-583X/$ - see front matter © 2008 Elsevier B.V. All rights reserved.
doi:10.1016/j.nimb.2008.11.008

been extensively used by many groups [12–18] to a variety of solids, including materials of biological interest [19–26]. There are generally two main problems with this methodology: (i) optical data are not always available or cover only a limited energy-loss range (this is especially true for biological materials) and (ii) due to the scarcity of experimental data beyond the optical limit (i.e. for finite momentum-transfer), the extension schemes used are often based on various simplifications of the Lindhard dielectric function (e.g. plasmon-pole approximation). The above issues become critical with decreasing electron energy where the IMFP becomes more and more sensitive to details of the dielectric response function. Hence, the extended-optical-data method is generally not considered trustworthy below 50–100 eV. On the other hand, first-principle calculations although more reliable are far less practical and, therefore, limited to very low energies (below ~20 eV) [7].

Despite being originally developed for the HEG, the Lindhard dielectric function often performs reasonably well in materials with a well-defined plasmon-like peak in their energy-loss spectrum [27]. Moreover, it has the advantage of automatically providing the extension to finite momentum-transfers, while being free of any empirical (or adjustable) parameters; the only material input needed is trivially obtained from the bulk electronic density of the material. Corrections to the Lindhard dielectric function are, in practice, of two kinds, namely, the (static) many-body local-field correction (LFC) for short-range exchange-correlation effects and damping corrections due to plasmon's finite lifetime. It should be noted that damping is a natural outcome of a dynamic LFC theory. In the present study, we use the full Lindhard dielectric function to calculate electron IMFPs for electron-gas densities representative of biological materials. The influence of the LFC is examined through the application of several widely used analytic approximations for its static limit. As a first approximation (and consistent with a static-LFC) damping effects are neglected to all orders. Comparisons are made against recent experiments and semi-empirical calculations.

2. Methodology

2.1. Inelastic mean free path (IMFP)

In the plane-wave first-Born approximation the IMFP (λ) of a non-relativistic electron of kinetic energy T is given by:

$$\lambda(T)=\frac{\pi a_o T}{\int dE \int \mathrm{Im}[-1/\varepsilon(E,q)]q^{-1}dq}, \tag{1}$$

where $\mathrm{Im}[-1/\varepsilon(E,q)]$ is the imaginary part of the inverse dielectric response function (the so-called energy-loss-function, ELF), q and E are the momentum and energy transfer in the inelastic collision, respectively, and a_o is the Bohr radius (0.0529 nm). The inelastic cross section in the conventional microscopic units of area per scattering center is simply $\sigma = 1/(n\lambda)$, where n is the density of scattering centers. A homogeneous and isotropic medium is assumed throughout, so q is a scalar quantity. The limits of integration are $q_{\pm}=\sqrt{2m}(\sqrt{T}\pm\sqrt{T-E})$ where m is the electron rest mass and $E_{\min} = E_G$, $E_{\max} = (T+E_G)/2$ where E_G is the band-gap energy. An analytic approximation to Eq. (1) is provided by Bethe's asymptotic expansion in powers of $1/T$ which reads [28]:

$$\lambda_{\mathrm{Bethe}}(T)=\frac{T}{A\ln T+B+CT^{-1}+O(T^{-2})}, \tag{2}$$

where the coefficients A, B and C are properties of the materials. Most importantly, the coefficient of the leading term (A) depends only on the optical limit of the ELF, i.e. $A\propto \mathrm{Im}[-1/\varepsilon(E,q=0)]$ which may be readily obtained from experiments. This realization is the basis of Bethe's high-energy (or optical) approximation: $\lambda_{\mathrm{Bethe}}(T)\approx T/(A\ln T)$. Analytic expressions of the form of Eq. (2) with adjustable material-dependent coefficients have been successfully used in fitting numerical results obtained from Eq. (1), most notable perhaps is NIST's predictive TPP formula [29].

2.2. The Lindhard dielectric function

Within a self-consistent time-dependent Hartree approximation (i.e. RPA) Lindhard [5] obtained an analytic expression for the dielectric function of the HEG which describes both single-particle (e.g. electron–hole pairs) and collective (plasmon) excitations. The Lindhard dielectric function accounts only for long-range correlation and, therefore, is exact only at the high-density limit ($n\to\infty$). If we write:

$$\varepsilon_L(E,q)=1+Q_0(E,q)=1+Q_0^R(E,q)+iQ_0^I(E,q), \tag{3}$$

where $\mathrm{Re}\,\varepsilon_L(E,q)=1+Q_0^R(E,q)$ and $\mathrm{Im}\,\varepsilon_L(E,q)=Q_0^I(E,q)$ are the real and imaginary parts of the Lindhard dielectric function (the subscript "0" denotes treatment at the RPA level), then the corresponding ELF reads:

$$\mathrm{Im}\left[\frac{-1}{\varepsilon_L(E,q)}\right]=\frac{Q_0^I(E,q)}{[1+Q_0^R(E,q)]^2+[Q_0^I(E,q)]^2}. \tag{4}$$

In notation convenient to the present study we can write:

$$\begin{aligned}Q_0^R(E,q)=\frac{4}{\pi q^2}(Ry/E_F)^{1/2}\times\Bigg\{&\frac{1}{2}+\frac{1}{4q}\left[1-\left(\frac{E+q^2}{2q}\right)^2\right]\\&\times\ln\left|\frac{E+2q+q^2}{E-2q+q^2}\right|+\frac{1}{4q}\left[1-\left(\frac{E-q^2}{2q}\right)^2\right]\\&\times\ln\left|\frac{E-2q-q^2}{E+2q-q^2}\right|\Bigg\}\end{aligned} \tag{5}$$

and

$$Q_0^I(E,q)=\begin{cases}\frac{E}{q^3}(Ry/E_F)^{1/2}, & \frac{E+q^2}{2q}<1\\ \frac{1}{q^3}(Ry/E_F)^{1/2}\left[1-\left(\frac{E-q^2}{2q}\right)^2\right], & \left|\frac{E-q^2}{2q}\right|<1<\frac{E+q^2}{2q}\\ 0, & 1<\left|\frac{E-q^2}{2q}\right|,\end{cases} \tag{6}$$

where Ry is the Rydberg constant (13.6 eV). The variables E and q in the right-hand-side of Eqs. (5) and (6) are, for compactness, expressed in units of the Fermi energy (E_F) and momentum (q_F), respectively. An important characteristic of the above expressions is that the only material property used is the electronic density (n) of the material through $q_F=\hbar(\alpha r_s\alpha_o)^{-1}$ and $E_F=(\alpha r_s)^{-2}\,Ry$ where $r_s=(4\pi n/3)^{-1/3}/a_o$ is the dimensionless electron-gas density parameter (or one-electron radius) and $\alpha=(4/9\pi)^{1/3}=0.521$.

The Lindhard dielectric function assumes an infinite plasmon lifetime (or zero plasmon linewidth). Thus, the plasmon excitation is represented by a Dirac delta function at the resonance energy $E_p=(12/r_s^3)^{1/2}Ry$ which, for q below some critical value q_c, shifts with momentum-transfer along a dispersion line E_p obtained by the condition $\mathrm{Re}\,\varepsilon_L(E,E_p(q))=0$. The value of q_c corresponds to the point where the plasmon dispersion line intersects the upper boundary of the single-particle region (see last condition in Eq. (6)). For $q>q_c$ the plasmon vanishes (zero lifetime) due its decay into electron–hole pairs. Thus, for electron energies below about twice (due to the Pauli principle) the plasmon energy, only electron–hole pairs contribute to $\varepsilon_L(E,q)$. This is an oversimplification for real materials which exhibit a finite plasmon linewidth for all q. Nevertheless, the Lindhard dielectric function is known to describe reasonably well the response of valence electrons in nearly-free-electron-like materials.

2.3. Local-field correction (LFC)

The many-body LFC (not to be confused with the crystal-LFC) is meant to account for short-range Coulomb-correlation and spin-exchange that are neglected in the RPA and which result in a local depletion of electron density around each screening electron (the so-called exchange-correlation hole). Then, the following expression would hold for the dielectric function of an *interacting* electron system [30]:

$$\varepsilon(E,q) = 1 + [\varepsilon_{\mathrm{RPA}}(E,q) - 1] \times \{1 - G(E,q)[\varepsilon_{\mathrm{RPA}}(E,q) - 1]\}^{-1}, \quad (7)$$

where $G(E,q)$ is the LFC which, in general, is a complex-value function depending on both the energy- and momentum-transfer. The imaginary part arises from the energy-dependence and leads to damping. Given the complexity of a dynamic treatment, we presently restrict our study to *static*-LFCs, i.e. we ignore the energy-dependence by assuming that $\mathrm{Im}\,G(E,q) = 0$ and $G(E,q) = \mathrm{Re}\,G(0,q) = G(q)$. Due to the weak energy-dependence of the LFC up to about twice the plasmon energy [7], the use of its static limit in IMFP calculations should be considered reliable at least up to ~100 eV electron energies (since $E_{\max} \approx T/2$ in Eq. (1)). In the present study, where the systems examined are approximated by a HEG we also set $\varepsilon_{\mathrm{RPA}}(E,q) = \varepsilon_L(E,q)$ in Eq. (7). Then, following the notation of the previous paragraph we can write:

$$\varepsilon(E,q) = 1 + \frac{Q_0(E,q)}{1 - G(q)Q_0(E,q)} \quad (8)$$

and

$$\mathrm{Im}\left[\frac{-1}{\varepsilon(E,q)}\right] = \frac{Q_0^I(E,q)}{\{1 + [1 - G(q)]Q_0^R(E,q)\}^2 + \{[1 - G(q)]Q_0^I(E,q)\}^2}. \quad (9)$$

Since the "exact" evaluation of the LFC is not possible (as this would involve solving the many-body problem), we can only hope for reliable yet tractable approximations. The importance of the LFC in understanding electron–electron interactions in condensed matter and, as a result, the excitation spectrum of materials, has resulted in a rich literature on the subject since the pioneering work of Hubbard in the late-50 s [31]. Having a closed-analytic form for $G(q)$ is particularly convenient for IMFP calculations through Eq. (1). Therefore, in the present study we have chosen to compare the performance of some widely used Hubbard-type LFCs which have a simple mathematical form, along with a more elaborated expression currently employed in many time-dependent density functional theory (TDDFT) calculations.

The first evaluation of $G(q)$ was made by Hubbard [31] who obtained by a diagrammatic technique a very simple approximation for the exchange correction while neglecting the correlation contribution. The Hubbard *exchange-only* LFC reads:

$$G_{\mathrm{H}}(q) = \frac{q^2}{2(q^2 + q_F^2)}. \quad (10)$$

In the literature, two alternative expressions are most often encountered. The Geldart and Vosko [32] modification consists in doubling the screening term so that the "*exact*" *exchange-only* LFC (within Hartree-Fock) at the limit $n \to \infty$ (or $r_s \to 0$) is obtained:

$$G_{\mathrm{GV}}(q) = \frac{q^2}{2(q^2 + 2q_F^2)}. \quad (11)$$

Another popular modification consists in adding an inverse screening length squared (q_s^2) in the denominator of Eq. (10) which would formally result if a screened (instead of a "bare") Coulomb potential is used in the Hartree-Fock evaluation of $G(q)$. Most often, this is expressed in terms of the Thomas-Fermi screening length, i.e. $q_s^2 = \zeta q_{TF}^2$ where ζ is a constant to be determined and $q_{TF}^2 = 4q_F/\pi a_o$. Here we follow Rice [33] and set $\zeta = 1$, so, the *screened-exchange-only* LFC reads:

$$G_{\mathrm{R}}(q) = \frac{q^2}{2(q^2 + q_F^2 + q_{TF}^2)}. \quad (12)$$

Eqs. (10)–(12) are meant to account only for the exchange-hole around each electron arising from Pauli's principle. Kleinman [34] and Langreth [35] showed that, in the static limit, the Coulomb-hole arising from short-range correlation may be accounted for using an expression similar to Eq. (12). Assuming again that $\zeta = 1$, the Kleinman–Langreth *exchange-correlation* LFC reads:

$$G_{\mathrm{KL}}(q) = \frac{q^2}{4[(q^2 + q_F^2 + q_{TF}^2) + (q_F^2 + q_{TF}^2)]}. \quad (13)$$

The Hubbard-type LFCs presented above are the ones most represented in the literature, although there seems to be no agreement as to the exact value of the parameter ζ or, more general, what this screening length should be. More refined analytic models do exist [36,37], but this comes generally with the expense of loosing the mathematical simplicity of the Hubbard-type expressions. Interest in LFCs has been revived since the advent of TDDFT. This is because the calculation of electronic excitations within TDDFT crucially depends upon the availability of good approximations for the exchange-correlation (xc) kernel $f_{xc}(E,q)$ of the HEG which is directly related to the LFC through [38]:

$$G(q) = -\frac{q^2}{4\pi} f_{xc}(E = 0, q). \quad (14)$$

At present, the most reliable analytic expressions for f_{xc} are considered those obtained from a parametrization of Quantum Monte-Carlo (QMC) data [39]. Among several such expressions, perhaps the most widely used in TDDFT calculations [40–43] is the CDOP formula [44] which provides an accurate representation of the latest QMC data of Moroni and co-workers [45] while also exhibiting the proper asymptotic behavior. It is also relatively simple which makes it very convenient for use in subsequent calculations of the type undertaken here. The CDOP expression for the *exchange-correlation* LFC reads:

$$G_{\mathrm{CDOP}}(q) = C(r_s)\left(\frac{q}{q_F}\right)^2 + \frac{B(r_s)q^2}{\gamma(r_s)q_F^2 + q^2} + \alpha(r_s)\left(\frac{q}{q_F}\right)^4 \exp\left[-\beta(r_s)\left(\frac{q}{q_F}\right)^2\right]. \quad (15)$$

Similar to the Hubbard-type expressions, Eq. (15) is a function of a single variable, namely, the electron density n which enters through the dimensionless coupling constant r_s. The other parameters relate to the asymptotic limits of $G(q)$ at small- and large-q. Keeping the same symbols with [44,45], $\alpha = 1.5A/(B\gamma r_s^{1/4})$, $\beta = 1.2/(B\gamma)$ and $\gamma = B/(A-C)$, where the A, B and C are found through:

$$\lim_{q\to 0} G(q) = A(r_s)\left(\frac{q}{q_F}\right)^2, \quad (16a)$$

$$\lim_{q\to \infty} G(q) = C(r_s)\left(\frac{q}{q_F}\right)^2 + B(r_s). \quad (16b)$$

The "exact" expressions for the above coefficients are [46]:

$$A(r_s) = \frac{1}{4} - \frac{1}{24}\left(\frac{4\pi^2}{9}\right)^{1/3}\left[r_s^3\frac{d^2E_c(r_s)}{dr_s^2} - 2r_s^2\frac{dE_c(r_s)}{dr_s}\right], \quad (17a)$$

$$C(r_s) = -\frac{\pi}{2q_F}\frac{d}{dr_s}[r_s E_c(r_s)], \quad (17b)$$

$$B(r_s) = \frac{2}{3}[1 - g(r=0)] + \frac{48}{35}\left(\frac{E_F}{E_p}\right)^2\delta_4 - \frac{16}{25}\left(\frac{E_F}{E_p}\right)^2(2\delta_2 + \delta_2^2), \quad (17c)$$

where E_c is the correlation energy per electron in a.u., $g(r)$ is the pair-distribution function for the HEG, that is, the probability of finding a pair of electrons at distance r from each other, δ_2 denotes the fractional change of the average electron kinetic energy due to correlation and δ_4 is the same for the squared kinetic energy. The most accurate evaluation of E_c is also obtained from QMC calculations. In the present study, we use the Perdew-Zunger (PZ) parametrization [47] which provides the best available fit to the QMC data of Ortiz and Ballone [48]. The PZ expression in the present density range ($r_s > 1$) reads (E_c in a.u.):

$$E_c(r_s) = \gamma(1 + \beta_1\sqrt{r_s} + \beta_2 r_s)^{-1}, \tag{18}$$

where $\gamma = -0.103756$, $\beta_1 = 0.56371$ and $\beta_2 = 0.27358$. From Eq. (18), the evaluation of Eqs. (17a) and (17b) follows in a straightforward manner. With respect to Eq. (17c), although reliable and simple expressions for both $g(r = 0)$ and δ_2 are available, the evaluation of δ_4 is particularly problematic since, being a second moment value, it is more sensitive to the details of electron correlation. It is therefore customary to obtain the parameter $B(r_s)$ from a fit to QMC data as well. The expression suggested in [45] reads:

$$B(r_s) = \frac{1 + \alpha_1 x + \alpha_2 x^3}{3 + b_1 x + b_2 x^3}, \tag{19}$$

where $x = \sqrt{r_s}$, $\alpha_1 = 2.15$, $\alpha_2 = 0.435$, $b_1 = 1.57$ and $b_2 = 0.409$. Calculations with the CDOP formula are then performed by inserting Eqs. (17a), (17b), (18) and (19) in Eq. (15).

3. Results and discussion

The only material parameter needed as input for the present calculations is the dimensionless electron-gas density parameter $r_s = (4\pi n/3)^{-1/3}/a_o$ or, after substituting the various constants, $r_s = (16.1 \times 10^{23}/n)^{1/3}$ where n is the electron density. For inelastic scattering calculations, it is customary to divide the electronic subsystem of the material into valence and inner shells. The valence-shell electrons with typical binding energies less than ~100 eV are assumed to exhibit an "electron-gas" behavior whereas the inner shells are assumed to retain their atomic character. In this representation, the value of n should be calculated based on the number of valence electrons only. In order to avoid an independent estimate of the inner shell contribution, a brute-force application of the electron-gas theory to *all* electrons in the system is also employed. This approximation should suffice for a comparative analysis between different LFC representations. Moreover, for biological materials where the number of inner shell electrons is relatively small compared to the total number, the error in the absolute magnitude of the IMFP is shown to be generally less than ~10%. In Table 1, we present the material parameters used in the present calculations.

In Fig. 1, we present for different values of momentum-transfer the real and imaginary parts of the dielectric response function of liquid water and solid-DNA. The calculations of Fig. 1 are based on Eqs. (5) and (6) where $\mathrm{Re}\,\varepsilon_L(E,q) = 1 + Q_0^R(E,q)$ and $\mathrm{Im}\,\varepsilon_L(E,q) = Q_0^I(E,q)$. In Fig. 2, the corresponding ELFs for the two materials

Table 1
Material parameters for water (H_2O), DNA ($C_{20}H_{27}N_7O_{13}P_2$ or $C_{19}H_{26}N_8O_{13}P_2$) and PMMA ($C_5H_8O_2$) used in the present electron-gas calculations. Values in the parenthesis correspond to valence electrons only.

	Water	DNA	PMMA
Mass density (ρ) in g/cm^3	1	1.35	1.19
Electron density (n) in cm^{-3} ($\times 10^{23}$)	3.34 (2.67)	4.12 (2.97)	3.86 (2.86)
One-electron radius (r_s)	1.69 (1.82)	1.58 (1.76)	1.61 (1.78)
Plasmon energy (E_p) in eV	21.4 (19.2)	23.8 (20.2)	23.1 (19.8)
Fermi energy (E_F) in eV	17.5 (15.1)	20.2 (16.2)	19.3 (15.8)

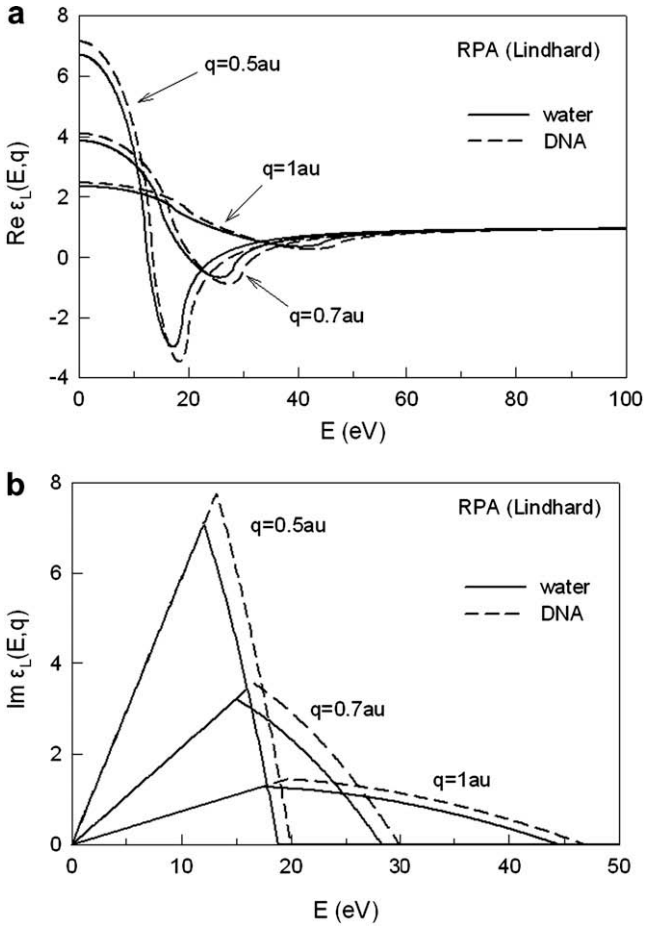

Fig. 1. Real and imaginary parts of the dielectric function of condensed-water and solid-DNA for different values of momentum-transfer calculated from the Lindhard dielectric function for density parameters $r_s = 1.69$ and $r_s = 1.58$, respectively.

are presented as calculated from Eqs. (3)–(6) for several values of momentum-transfer. For the smallest momentum-transfer ($q = 0.5$ a.u.), one can recognize the sharp plasmon peak at the resonance energy predicted by the RPA dispersion relation which, up to 2nd order in q, reads: $E_p(q) = E_p(q = 0) + 1.276 r_s^{-1/2} q^2 Ry$ (E and Ry in eV; q in a.u.). For $q = 0.5$ a.u., the plasmon energies are about 24.8 eV and 27.3 eV for water and DNA, respectively. The plasmon contribution to the ELF, although formally being a Dirac delta function, can be practically reproduced by expanding (as a power series in q) $\mathrm{Re}\,\varepsilon_L(E,q)$ about the plasmon energy and taking $\mathrm{Im}\,\varepsilon_L(E,q)$ to be a very small number. For the higher values of q depicted in Fig. 2, the plasmon peak vanishes due its decay into single-particle excitations. Mathematically, this trivially follows from the condition $E_p(q) < q^2 Ry + 2q(E_F Ry)^{1/2}$ of Eq. (6). In more advanced theories [50], the plasmon peak never vanishes, but simply broadens with increasing q. In the case of liquid water, the momentum broadening of $\mathrm{Im}[-1/\varepsilon(E,q)]$ has been considered only recently via the Mermin modification of Lindhard dielectric function [51], or by implementing a momentum-dependent damping coefficient in an extended Drude dielectric model [51,52]. Both descriptions are shown to substantially improve the agreement with experimental data at finite momentum-transfer [51,52].

The dependence of the LFC on momentum-transfer is presented in Fig. 3 for the different models examined (see Eqs. (10), (11), (12), (13), and (15)). All models exhibit a common trend at very small q which, following Eq. (16a), corresponds to the theoretically expected asymptotic limit $G(q \to 0) \approx q^2$. However, with increasing q a different behavior is observed depending on whether correla-

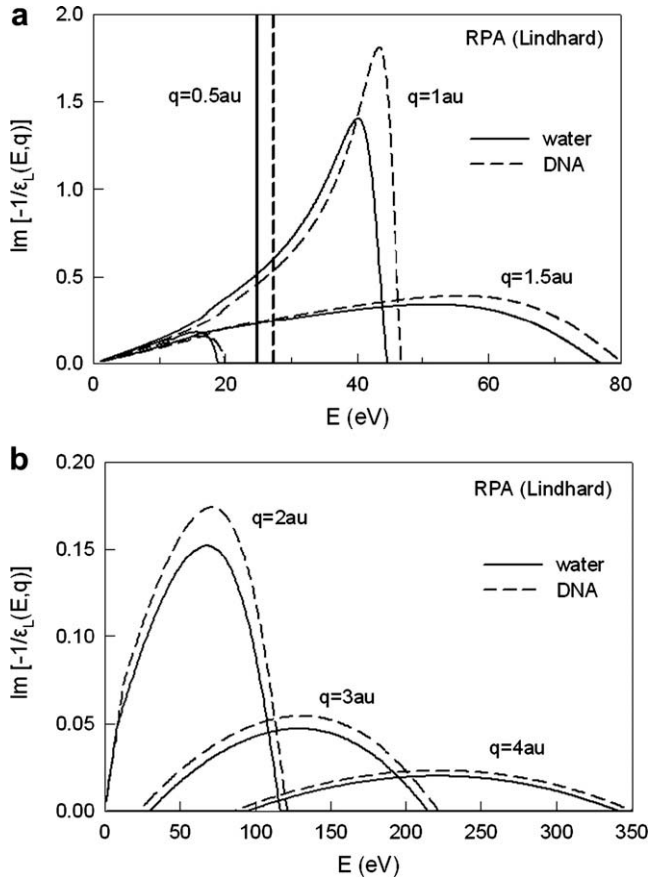

Fig. 2. Energy-loss-function (ELF) for different values of momentum-transfer corresponding to the dielectric functions of Fig. 1.

tion is considered. Specifically, the models that account for exchange-only (H, GV, R) reach a plateau and asymptotically approach the value $G(q \to \infty) \approx 1/2$. On the other hand, the models that account for both exchange and correlation (KL and CDOP) exhibit a continuous rise. As can be seen from Eq. (17b), when correlation is taken into account the parameter C takes a non-zero value leading to the high-q asymptotic limit $G(q \to \infty) \approx q^2$.

In Fig. 4, the momentum-dependence of the ELF for the different LFC models is presented. The influence of the LFC is sizeable resulting in the enhancement of the ELF spectrum at small energy-losses. This is due to a lower dispersion coefficient compared to the RPA

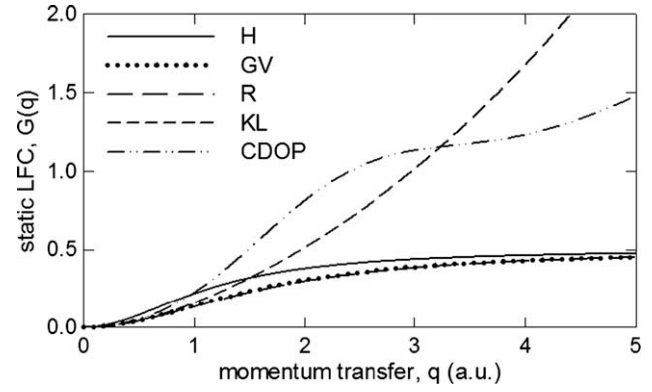

Fig. 3. Static local-field-correction (LFC) as function of momentum-transfer for the various models considered (H: Hubbard, GV: Geldart and Vosko, R: Rice, KL: Kleinman and Langreth, CDOP: Corradini, Del Sole, Onida, Palumno).

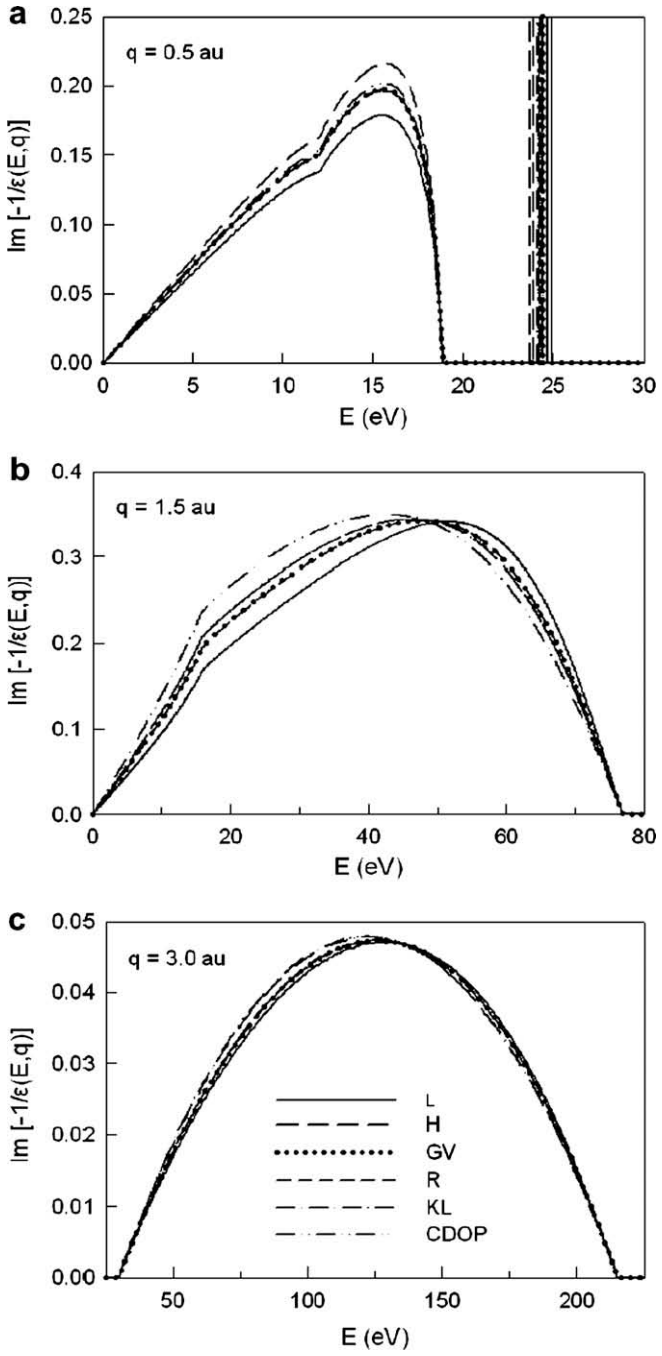

Fig. 4. Momentum-dependence of the ELF for the different LFC models presented in Fig. 3 plus the Lindhard ELF (L).

value: $\alpha_{\rm LFC} = \alpha_{\rm RPA} - 0.470 r_s^{1/2} A_{\rm LFC}(r_s)$ where $\alpha_{\rm RPA} = 1.276 r_s^{-1/2}$ and the factor $A_{\rm LFC}(r_s)$ for each LFC model is obtained from Eq. (16a). The effect gradually vanishes with increasing momentum-transfer since $Q_0^R(E,q), Q_0^I(E,q) << 1$ for large E.

The performance of the Lindhard dielectric function with and without an LFC, to electron IMFP calculations in materials of biological interest is examined in Figs. 5 and 6. For a meaningful comparison, all results presented in the figures are based on the plane-wave first-Born approximation (Eq. (1)). In Fig. 5, we compare the present calculations using the Lindhard dielectric function (without LFC), against some other model calculations which are based on the extended-optical-data dielectric methodology. Results are shown for liquid water (panel a), DNA (panel b) and

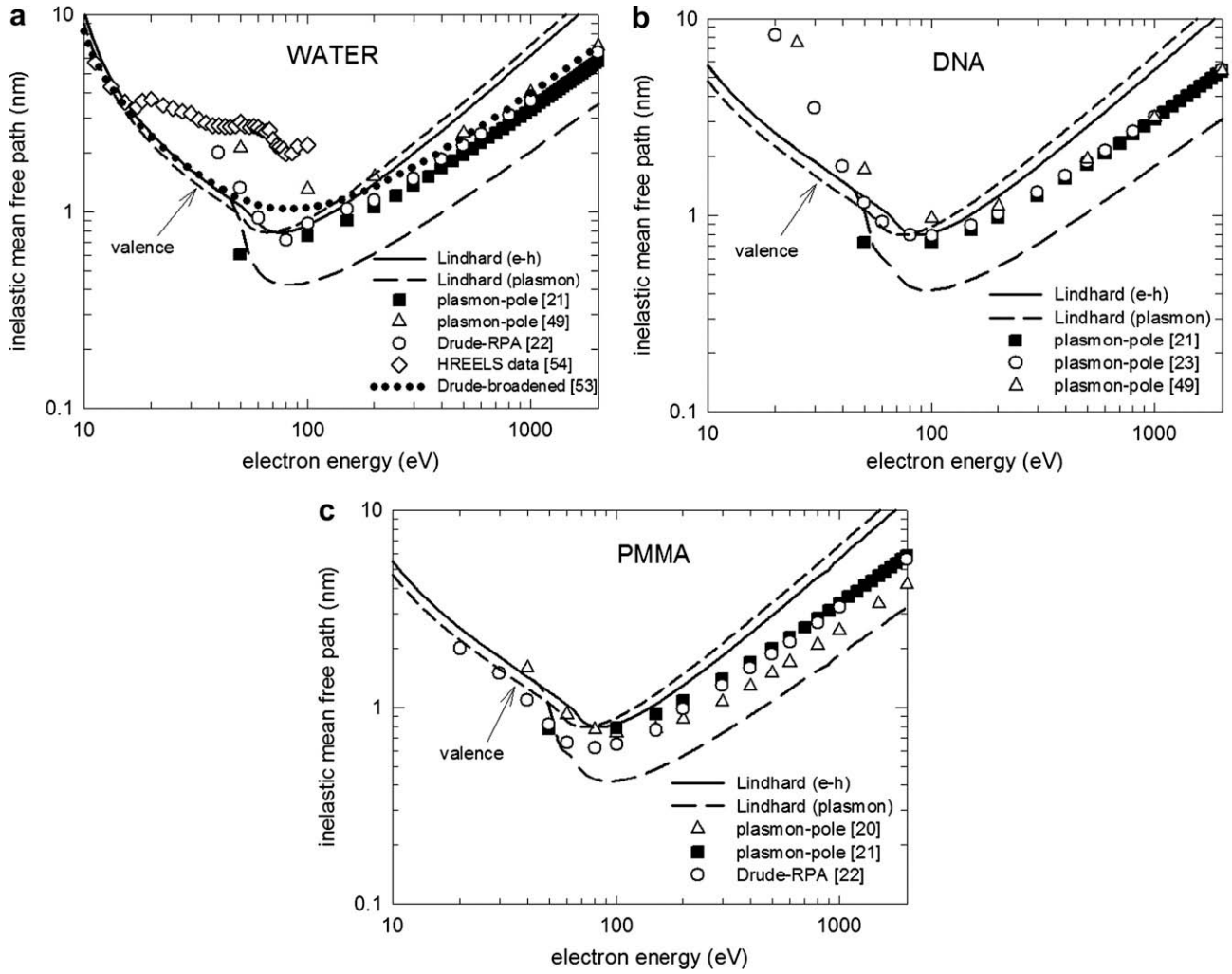

Fig. 5. Electron inelastic mean free paths (IMFP) in (a) condensed-water, (b) solid-DNA and (c) PMMA using various approximations for the dielectric response function. All calculation results presented are based on the plane-wave first-Born approximation. The experimental data of Michaud et al. [54] are based on high-resolution-electron-energy-loss-spectroscopy. The e–h and plasmon contribution of the Lindhard dielectric function to the IMFP is explicitly shown. For the e–h contribution calculations are shown using both the valence and total electron-gas density parameters.

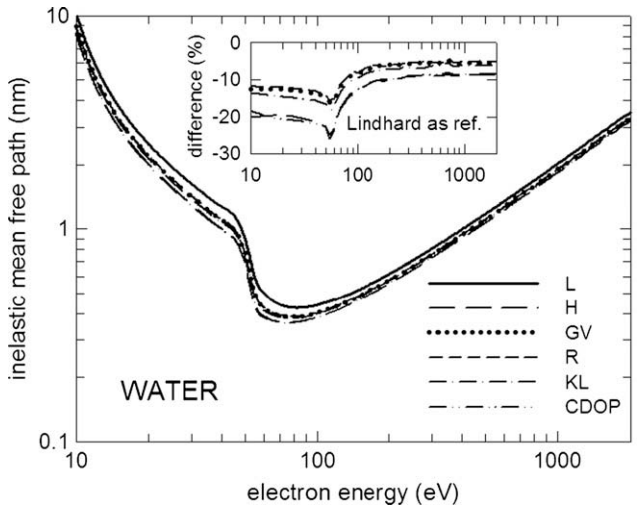

Fig. 6. Effect of different LFC models upon the electron IMFPs in the case of condensed-water. The notation is the same with Figs. 3 and 4. The inset shows the difference (in %) with respect to the Lindhard-ELF.

PMMA (panel c). The plasmon and e–h contribution to the IMFP is explicitly shown. The magnitude of the e–h contribution based on the valence electron density is also included. The comparison, which is by no means exhaustive, is sufficient to provide important insight upon the effect of the various model approximations adopted in the calculation of the IMFP in the context of the dielectric methodology. The discussion will be divided into the region above and below the IMFP minimum ($\sim$100 eV).

For energies above the IMFP minimum, the e–h contribution alone significantly overestimates the semi-empirical IMFP calculations. The addition of the plasmon contribution brings a substantial decrease to IMFP which becomes now too small; a consequence of the assumption of an undamped plasmon in the Lindhard dielectric function (see also below). The use of the valence electron density instead of the total electron density causes a $\sim$10% increase of the IMFP. However, in this case the inner shell contribution must be added independently by some other model calculation which will cause a corresponding decrease of the IMFP. Therefore the error made by the brute-force application of the electron-gas approximation is expected to be less than $\sim$10%. The overall good agreement among the semi-empirical dielectric calculations in this range must be attributed to the use of a experimental ELF data at $q \approx 0$ since they all employ different dispersion schemes for the

extension of the dielectric response function to finite momentum-transfer ($q > 0$). This is in accord to the predictions of the Bethe asymptote (Eq. (2)) whereby at sufficiently high projectile energies the IMFP is largely determined by the optical limit of the ELF (Bethe's optical approximation).

The situation is different below the IMFP minimum since, at the low-energy region (<100 eV), the momentum-dependence of the dielectric response function becomes critical. The plasmon-pole model used, among others, by the NIST group, gradually deteriorates in this range due to its very simplistic dispersion which, essentially, collapses the whole ELF spectrum to a delta-like peak with increasing momentum-transfer [49]. In effect, this yields an ELF spectrum whose width is too narrow and whose height is too large [51]. The situation is somewhat improved when the Drude-RPA model is used. In this approximation, the optical-ELF is represented by a linear combination of Drude-type functions which are extended to $q > 0$ by implementing an RPA quadratic dispersion (but with $\alpha_{RPA} = 1$). In contrast to the plasmon-pole model though, the Drude-RPA model does retain some broadened structure for the ELF at $q > 0$ through its damping constant (which is not dispersed) [51]. Further improvement is obtained by the extended Drude model of Emfietzoglou and co-workers [51–53] which empirically accounts for local-field effects and the dispersion of the damping constant. These improvements lead to momentum broadening and shifting of the plasmon peak resulting in very good agreement with the experimental ELF of liquid water at both zero and finite momentum-transfers [51–53]. With decreasing electron energy (<50 eV) the IMFP calculated from the Lindhard dielectric function approaches the more accurate calculations [26] as well as the experimental HREELS data [54]. This is an important finding given that below 50–100 eV the majority of semi-empirical dielectric calculations become increasingly inaccurate. The reason for this is that the semi-empirical dielectric models of the plasmon-pole or Drude-RPA type essentially neglect the momentum broadening of the ELF. Eventually, at low electron energies, a situation is encountered where the ELF is either entirely (plasmon-pole models) or for the most part (Drude-RPA models) outside the integration limits of momentum-transfer in Eq. (1). Note that the lack of momentum broadening in the above models is also accompanied by an incorrect peak position due to the neglect of local-field effects which further worsens the above situation. In contrast, at very low electron energies (below about twice the plasmon energy), the e–h contribution of the Lindhard dielectric function already provides a reasonable (albeit very simplistic) representation of the energy-loss spectrum through its broadened e–h structure. As we have shown recently [51], the effect of damping can be reasonably accounted in the context of Lindhard theory by Mermin's prescription [50] which is expected to further improve the performance of the electron-gas calculations. It is worth noting that the brute-force application of the electron-gas approximation in the Lindhard calculations, which is clearly invalid for energies below the inner shell edges (<100 eV), affects the absolute values of the IMFPs by less than ~15% for all materials examined. Specifically, in the case where the valence electron densities are being used, the plasmon energies becomes smaller by 1–2 eV causing an increase of inelastic scattering cross sections at low electron energies and a corresponding decrease of IMFPs.

In Fig. 6, we show the effect of the examined LFCs upon the electron IMFPs in the case of liquid water. The LFC reduces the IMFP by ~5–10% above 100 eV and by ~10–30 % below 100 eV. The highest reduction is obtained by the CDOP and original Hubbard models. Surprisingly, the very simple Hubbard formula leads to almost identical results (±1–2%) with the more accurate CDOP expression. It follows that the high-q behaviour of $G(q)$ is practically inconsequential to IMFP calculations. The present findings with respect to the magnitude of the IMFP reduction, are in very good agreement with those of Ashley and co-workers [55] for the case of aluminum. Those authors, however, limited their study to the original Hubbard formula. More recently, using an LFC derived from the local-density-approximation (equivalent to Eq. (16a)), Echenique and co-workers [7] reported a reduction by ~20% of hot-electron lifetimes (and thus IMFP) for energies a few eV above the Fermi level, in good agreement with our low-energy estimates. Also, in a comprehensive study on the effect of LFCs upon the electron-gas stopping-power, Pathak and Yussouff [56] found a small effect (few %) which agrees with our conclusions above 100 eV. On the other hand, Penn [57] found that in the 0.2–2 keV electron range the LFC leads to an increase of the IMFP by 10–20%. However, Penn used the plasmon-pole approximation and not the full Lindhard dielectric function in his calculations.

4. Conclusion

The present study shows that the Lindhard dielectric function which is free from any adjustable parameters may provide reasonable estimates of electron IMFPs in biological materials below ~50 eV via its e–h contribution. In this very low-energy region the majority of semi-empirical dielectric calculations based on the extended-optical-data methodology with an (uncorrected) RPA dispersion are known to fail. The use of the LFC results in a sizeable reduction of IMFPs which, for electron energies below 100 eV, may reach ~20%. The present calculations can be further improved by (i) using a dynamic (instead of static) LFC, (ii) adding corrections to the plane-wave Born approximation and (iii) accounting for the exchange-hole around both the incident and scattering electron (related to the so-called vertex corrections). It is expected that any of the above improvements will decrease the inelastic scattering cross section and, correspondingly, increase the IMFP bringing better agreement with experimental data.

Acknowledgments

DE and IK acknowledge financial support by the European Union FP7 ANTICARB (HEALTH-F2-2008-201587) research programme and by an internal grand from the Research Committee of the University of Ioannina (Grant No. 80037). IA and RGM acknowledge financial support by the Spanish Ministerio de Educación y Ciencia (Projects FIS2006-13309-C02-01 and FIS2006-13309-C02-02).

References

[1] W.S.M. Werner, Surf. Interface Anal. 31 (2001) 141.
[2] B. Ziaja, R.A. London, J. Hajdu, J. Appl. Phys. 97 (2006) 064905-1.
[3] H. Nikjoo, S. Uehara, D. Emfietzoglou, F.A. Cucinotta, Radiat. Meas. 41 (2006) 1052.
[4] M. Reigrotzki, R. Redmer, N. Fitzer, S.M. Goodnick, M. Dur, W. Schattke, J. Appl. Phys. 86 (1999) 4458.
[5] J. Lindhard, Kgl. Dansk. Vid. Mat. Fys. Medd. 28 (1954) 1.
[6] G. Onida, L. Reining, A. Rubio, Rev. Mod. Phys. 74 (2002) 601.
[7] P.M. Echenique, J.M. Pitarke, E.V. Chulkov, A. Rubio, Chem. Phys. 251 (2000) 1.
[8] J.M. Pitarke, I. Campillo, Nucl. Instr. and Meth. B 164 (2000) 147.
[9] A.P. Sorini, J.J. Kas, J.J. Rehr, M.P. Prange, Z.H. Levine, Phys. Rev. B 74 (2006) 165111-1.
[10] C.J. Powell, A. Jablonski, J. Phys. Chem. Ref. Data 28 (1999) 19.
[11] J.M. Fernandez-Varea, F. Salvat, M. Dingfelder, D. Liljequist, Nucl. Instr. and Meth. B 229 (2005) 187.
[12] J.C. Ashley, J.J. Cowan, R.H. Ritchie, Thin Solid Films 60 (1977) 361.
[13] S. Tanuma, C.J. Powell, D.R. Penn, Surf. Interface Anal. 11 (1988) 577.
[14] S. Tougaard, Solid State Commun. 61 (1987) 547.
[15] Z.-J. Ding, R. Shimizu, Surf. Sci. 222 (1989) 313.
[16] J.-Ch. Kuhr, H.-J. Fitting, Phys. Stat. Sol. A 172 (1999) 433.
[17] A. Akkerman, T. Boutboul, A. Breskin, R. Chechik, A. Gibrekhterman, Y. Lifshitz, Phys. Stat. Sol. B 198 (1996) 769.
[18] I. Abril, R. Garcia-Molina, C.D. Denton, J. Pérez-Pérez, N.R. Arista, Phys. Rev. A 58 (1998) 357.
[19] B. Ziaja, A. Szoke, D. van der Spoel, J. Hadju, Phys. Rev. B 66 (2002) 024116.
[20] J.C. Ashley, J. Electron Spectrosc. Relat. Phenom. 28 (1982) 177.

[21] S. Tanuma, C.J. Powell, D.R. Penn, Surf. Interface Anal. 21 (1993) 165.
[22] A. Akkerman, E. Akkerman, J. Appl. Phys. 86 (1999) 5809.
[23] Z. Tan, Y. Xia, M. Zhao, X. Liu, F. Li, B. Huang, Y. Li, Nucl. Instr. and Meth. B 222 (2004) 27.
[24] N. Timneanu, C. Caleman, J. Hadju, D. van der Spoel, Chem. Phys. 299 (2004) 277.
[25] M. Dingfelder, D. Hantke, M. Inokuti, H.G. Paretzke, Radiat. Phys. Chem. 53 (1998) 1.
[26] D. Emfietzoglou, H. Nikjoo, Radiat. Res. 163 (2005) 98.
[27] D.R. Penn, Phys. Rev. B 35 (1987) 482.
[28] M. Inokuti, Rev. Mod. Phys. 43 (1971) 297.
[29] S. Tanuma, C.J. Powell, D.R. Penn, Surf. Interface Anal. 35 (2003) 268.
[30] S. Ichimaru, Rev. Mod. Phys. 54 (1982) 1017.
[31] J. Hubbard, Proc. R. Soc. Lond. A 243 (1958) 336.
[32] D.J.W. Geldart, S.H. Vosko, Can. J. Phys. 44 (1966) 2137.
[33] T.M. Rice, Ann. Phys. 31 (1965) 100.
[34] L. Kleinman, Phys. Rev. 160 (1967) 585.
[35] D.C. Langreth, Phys. Rev. 181 (1969) 753.
[36] S. Ichimaru, K. Utsumi, Phys. Rev. B 24 (1981) 7385.
[37] P. Vashishta, K.S. Singwi, Phys. Rev. B 6 (1972) 875.
[38] S. Botti, A. Schindlmayr, R. Del Sole, L. Reining, Rep. Prog. Phys. 70 (2007) 357.
[39] S. Hellal, J.-G. Gasser, A. Issolah, Phys. Rev. B 68 (2003) 094204-1.
[40] V. Olevano, M. Palumno, G. Onida, R. Del Sole, Phys. Rev. B 60 (1999) 14224.
[41] M. Lein, E.K.U. Gross, J.P. Perdew, Phys. Rev. B 61 (2000) 13431.
[42] G.E. Simion, G.F. Giuliani, Phys. Rev. B 77 (2008) 035131-1.
[43] L.A. Constantin, J.M. Pitarke, Phys. Rev. B 75 (2007) 245127-1.
[44] M. Corradini, R. Del Sole, G. Onida, M. Palumno, Phys. Rev. B 57 (1998) 14569.
[45] S. Moroni, D.M. Ceperley, G. Senatore, Phys. Rev. Lett. 75 (1995) 689.
[46] J. Toulouse, Phys. Rev. B 72 (2005) 035117-1.
[47] J.P. Perdew, A. Zunger, Phys. Rev. B 23 (1981) 5048.
[48] G. Ortiz, P. Ballone, Phys. Rev. B 50 (1994) 1391.
[49] J.A. LaVerne, S.M. Pimblott, Radiat. Res. 141 (1995) 208.
[50] N.D. Mermin, Phys. Rev. B 1 (1970) 2362.
[51] D. Emfietzoglou, I. Abril, R. Garcia-Molina, I.D. Petsalakis, H. Nikjoo, I. Kyriakou, A. Pathak, Nucl. Instr. and Meth. B 266 (2008) 1154.
[52] D. Emfietzoglou, F. Cucinotta, H. Nikjoo, Radiat. Res. 164 (2005) 202.
[53] D. Emfietzoglou, H. Nikjoo, Radiat. Res. 167 (2007) 110.
[54] M. Michaud, A. Wen, L. Sanche, Radiat. Res. 159 (2003) 3.
[55] J.C. Ashley, C.J. Tung, R.H. Ritchie, Surf. Sci. 81 (1979) 409.
[56] A.P. Pathak, M. Yussouff, Phys. Stat. Sol. B 49 (1972) 431.
[57] D.R. Penn, Phys. Rev. B 13 (1976) 5248.